Editors' Suggestion

Effects of non-Hermitian perturbations on Weyl Hamiltonians with arbitrary topological charges

Alexander Cerjan, Meng Xiao, Luqi Yuan, and Shanhui Fan
Department of Electrical Engineering, and Ginzton Laboratory, Stanford University, Stanford, California 94305, USA

(Received 6 December 2017; published 13 February 2018)

We provide a systematic study of non-Hermitian topologically charged systems. Starting from a Hermitian Hamiltonian supporting Weyl points with arbitrary topological charge, adding a non-Hermitian perturbation transforms the Weyl points to one-dimensional exceptional contours. We analytically prove that the topological charge is preserved on the exceptional contours. In contrast to Hermitian systems, the addition of gain and loss allows for a new class of topological phase transition: when two oppositely charged exceptional contours touch, the topological charge can dissipate without opening a gap. These effects can be demonstrated in realistic photonics and acoustics systems.

DOI: 10.1103/PhysRevB.97.075128

I. INTRODUCTION

The study of topological systems represents an important frontier in both condensed-matter physics and photonics, as these systems can possess exotic electronic and photonic states, such as chiral surface states, which realize nonreciprocal transport [1–15]. A defining feature of these unusual topological states is their protection against many forms of disorder.

One important class of three-dimensional topological systems are Weyl semimetals [16–30], which possess a set of isolated degeneracies in their band structure. These degeneracies possess topological charges and represent sources or sinks of Berry flux [31]. It is known that in a system with Weyl points, any Hermitian perturbation can only change the location of the Weyl points and cannot remove or create them. Such Hermitian perturbations are common in electronic systems. On the other hand, in photonic systems there are many perturbations, such as material gain and absorption, as well as radiative outcoupling, which break hermiticity. Moreover, many recent studies have indicated that introducing non-Hermitian perturbations in topologically trivial systems can result in unusual phenomena, such as promoting single mode operation in lasers [32–38], loss-induced transmission in waveguide arrays [39,40], reverse pump dependence in lasers [41–43], and control over pairs of polarization states [44,45]. Analogously, therefore, it is important to understand how non-Hermitian perturbations influence the properties of topologically nontrivial systems [46–54].

In previous studies of topologically trivial periodic systems, it was discovered that when a non-Hermitian perturbation is introduced, degeneracies in the band structure of the underlying Hermitian system can transform to rings of exceptional points where both the eigenvalues and eigenvectors become identical, and the system has a nontrivial Jordan normal form [55–63]. More recently, it was discovered that starting from a Hermitian system supporting charge-1 Weyl points, which is a topologically nontrivial degeneracy, introducing a non-Hermitian perturbation can transform a Weyl point into an exceptional ring, with the Berry charge of the original Weyl point preserved on the ring [51,54]. Integrating the Berry curvature on a surface surrounding the exceptional ring yields a quantized Berry charge, while integrating the Berry curvature on a surface inside the exceptional ring yields no charge. All of these studies point to the connection between degeneracies in Hermitian systems, and the creation of exceptional rings when such systems are subject to non-Hermitian perturbations. However, there has not been a general treatment of the effects of breaking the hermiticity of Weyl points with an arbitrary charge, nor a systematic approach to the unusual properties of these exotic systems.

In this paper, we provide a systematic study of non-Hermitian topologically charged systems. Our study uncovers a set of remarkable effects in this class of systems. First, we analytically prove that in the presence of arbitrary non-Hermitian perturbation, a Weyl point with an arbitrary charge also transforms into a closed one-dimensional exceptional contour, with the topological charge preserved on the contour. However, such a contour need not form a single ring, but it can take a more complex shape when the charge is greater than 1. Second, we demonstrate that, in contrast to Hermitian systems, the addition of gain and loss allows for an alternative mechanism by which the topological charge in the system can dissipate: when two oppositely charged exceptional contours touch, the resulting exceptional contour does not possess a Berry charge. Unlike a Hermitian system, here the disappearance of the charge is not associated with the opening of the band gap. Third, in such systems the upper and lower bands associated with the exceptional ring are two branches of the same Riemann sheet, and so it is possible to follow a smooth path through the exceptional contour and transition from being on the upper band to being on the lower band. Finally, all of these effects can be demonstrated in realistic photonic and acoustic systems.

The remainder of this paper is organized as follows. In Sec. II, we present a general theoretical treatment using an effective two-band Hamiltonian. In particular, Sec. II B provides the analytic proof of the conservation of topological charge on the exceptional contour, and Sec. II D describes how the addition of gain and loss can dissipate topological charge. In Sec. III we observe a pair of charge-2 Weyl

points that transform into nonring exceptional contours in a tight-binding model of a photonic system. In Sec. IV we discuss the effects of gain and loss on the chiral edge modes of a system. Finally, we offer some concluding remarks in Sec. V.

II. MODELS OF NON-HERMITIAN TOPOLOGICAL SYSTEMS

A. Formation of exceptional contours from charge-*n* Weyl points

One of the most important differences between Hermitian and non-Hermitian systems are the types of eigenvalue degeneracies that each system type displays. Although both systems can display ordinary degeneracies where two or more eigenvalues become equal, non-Hermitian systems can also possess exceptional points, where not only are the eigenvalues equal, but the eigenvectors become identical and self-orthogonal, and the system has a nontrivial Jordan normal form [64–66].

In spite of the differences, there is in fact a general connection between the band degeneracies in Hermitian systems and the exceptional points when a non-Hermitian perturbation is added to such systems [59,60,67]. To illustrate this connection in topologically nontrivial systems, we first consider a general three-dimensional Hermitian system with a charge-n Weyl point. The 2×2 Hamiltonian in the vicinity of such a Weyl point has the form [68]

$$H(\mathbf{k}) = k_+^n \sigma_+ + k_-^n \sigma_- + k_z \sigma_z + \omega_0 I, \tag{1}$$

in which $k_\pm = (k_x \pm i k_y)$, $\sigma_\pm = 1/2(\sigma_x \pm i\sigma_y)$, $\sigma_{x,y,z}$ are the Pauli matrices, I is the 2×2 identity matrix, and ω_0 is the frequency of the Weyl point. In the vicinity of the Weyl point, the two bands are described by

$$\lambda_\pm = \omega_0 \pm \sqrt{\left(k_x^2 + k_y^2\right)^n + k_z^2}. \tag{2}$$

To achieve a degeneracy for which $\lambda_+ = \lambda_-$, we must have $k_x = k_y = k_z = 0$. This is an example of the general result that in a Hermitian system, three constraints must be simultaneously satisfied to achieve an accidental degeneracy in a system, i.e., a degeneracy that is not protected by a symmetry in the system [31,69]. As a result, for a Hermitian system in three-dimensional space, absent symmetry, degeneracies can only be found at isolated points in k-space.

We now add a generic non-Hermitian term to the previous Hamiltonian from Eq. (1), so that

$$H(\mathbf{k}) = k_+^n \sigma_+ + k_-^n \sigma_- + k_z \sigma_z + \omega_0 I + i\boldsymbol{\tau} \cdot \boldsymbol{\sigma}, \tag{3}$$

in which $\boldsymbol{\tau} = (\tau_x, \tau_y, \tau_z) \in \mathbb{R}$, $\boldsymbol{\sigma} = (\sigma_x, \sigma_y, \sigma_z)$, and we now allow ω_0 to be complex. Equation (3) yields a band structure of

$$\lambda_\pm(\mathbf{k}) = \omega_0 \pm \left\{k_\rho^{2n} + k_z^2 - \boldsymbol{\tau}^2 + 2i\left[\tau_x k_\rho^n \cos(n\phi) - \tau_y k_\rho^n \sin(n\phi) + \tau_z k_z\right]\right\}^{1/2}, \tag{4}$$

in which we have adopted cylindrical coordinates, (k_ρ, ϕ, k_z), with $k_\pm = k_\rho e^{\pm i\phi}$. In contrast to the Hermitian system, there are now only two criteria that must be met to find $\lambda_+ = \lambda_-$,

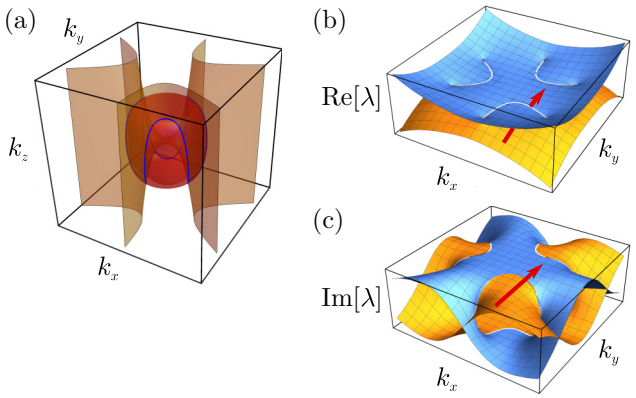

FIG. 1. (a) Exceptional contour associated with a charge-3 Weyl point under non-Hermitian perturbation, as described by Eq. (3) with $n = 3$ and $\boldsymbol{\tau} = (1,0,0.3)$. The two surfaces plotted are Eq. (5) (red) and Eq. (6) (orange), and their intersection defines the exceptional contour (blue). (b) Real parts of $\lambda_\pm$, Eq. (4), are shown in blue and yellow, respectively. (c) Imaginary parts of $\lambda_\pm$, Eq. (4), are shown in blue and yellow, respectively. In both (b) and (c), the red arrow indicates a smooth trajectory across the corresponding Riemann surface. It starts on the lower branch and ends on the upper branch.

$$0 = \left(k_x^2 + k_y^2\right)^n + k_z^2 - \boldsymbol{\tau}^2, \tag{5}$$

$$0 = \tau_x k_\rho^n \cos(n\phi) - \tau_y k_\rho^n \sin(n\phi) + \tau_z k_z. \tag{6}$$

Equations (5) and (6) define a single closed contour of degeneracies in $\mathbf{k}$ space. To prove that this contour consists entirely of exceptional points, we calculate the inner product of the right eigenvectors, $H|\psi_\pm^R\rangle = \lambda_\pm|\psi_\pm^R\rangle$, and left eigenvectors, $\langle\psi_\pm^L|H = \lambda_\pm\langle\psi_\pm^L|$,

$$\langle\psi_\pm^L|\psi_\pm^R\rangle = 2(\lambda_\pm - \omega_0)(\lambda_\pm - \omega_0 + k_z + i\tau_z), \tag{7}$$

which is necessarily zero on this degenerate contour, demonstrating that the eigenstates become self-orthogonal, one of the signatures of being at an exceptional point [64–66]. Therefore, we see that a topologically charged point degeneracy in a Hermitian system gives rise to a contour of exceptional points when a non-Hermitian perturbation is added. An example of an exceptional contour existing at the intersection of the two surfaces given in Eqs. (5) and (6) is shown in Fig. 1(a) for $n = 3$.

As $\lambda_\pm(\mathbf{k})$ is a multivalued complex function in non-Hermitian systems, the $\pm$ signs in Eq. (4) identify the two distinct branches of this function. Alternatively, one can view the two branches as being a part of the same Riemann surface, and we rewrite Eq. (4) as

$$\lambda_\theta(\mathbf{k}) = \omega_0 + \sqrt{a(\mathbf{k})}e^{i\theta/2}, \tag{8}$$

in which

$$\cos(\theta) = \frac{k_\rho^{2n} + k_z^2 - \boldsymbol{\tau}^2}{a(\mathbf{k})}, \tag{9}$$

$$\sin(\theta) = \frac{2\left[\tau_x k_\rho^n \cos(n\phi) - \tau_y k_\rho^n \sin(n\phi) + \tau_z k_z\right]}{a(\mathbf{k})}, \tag{10}$$

$$a(\mathbf{k}) = \Big[\big(k_\rho^{2n} + k_z^2 - \boldsymbol{\tau}^2\big)^2 + 4\big[\tau_x k_\rho^n \cos(n\phi) - \tau_y k_\rho^n \sin(n\phi) + \tau_z k_z\big]^2\Big]^{1/2}, \tag{11}$$

so that $\lambda_\theta(\mathbf{k})$ only returns to its original value for $\theta \to \theta + 4\pi$. The fact that the two bands constitute different branches of the same Riemann surface has a physical consequence. If one starts with a state on the lower band and travels through the exceptional contour where the upper and lower branches meet, the state smoothly transitions to being on the upper band. An example of this process can be seen in Figs. 1(b) and 1(c), where the red arrow marks a smooth trajectory across the Riemann surface, which exists on both branches of $\lambda_\pm$. As we will demonstrate in Sec. IV, this effect can also be seen in the projection of the bulk bands of semi-infinite systems.

B. Topological charge of an exceptional contour

To define a topological charge for the exceptional contour, the Berry connection, $\mathbf{A}(\mathbf{k})$, and Berry curvature, $\boldsymbol{\Omega}(\mathbf{k})$, must be generalized to non-Hermitian systems, for which the left and right eigenvectors are not necessarily related by the conjugate transpose, i.e., $\langle\psi^L| \neq (|\psi^R\rangle)^\dagger$. Although there are four reasonable possibilities for generalizing the Berry connection, which correspond to using different combinations of the left and right eigenstates in the definition

$$\mathbf{A}^{(L/R),(L/R)} = i\langle\psi^{(L/R)}(\mathbf{k})|\nabla_{\mathbf{k}}|\psi^{(L/R)}(\mathbf{k})\rangle, \tag{12}$$

Shen *et al.* have proven that the total Berry charge is the same for these four possibilities [54]. Thus, here we compute the local Berry curvature $\boldsymbol{\Omega}(\mathbf{k}) = \nabla_{\mathbf{k}} \times \mathbf{A}(\mathbf{k})$ for the λ_+ band of non-Hermitian system in Eq. (3) as

$$\Omega_\rho^{LR} = \left(\frac{n k_\rho^{n-1}}{2(\lambda - \omega_0)^3}\right)\big[k_\rho^n + i\tau_x \cos(n\phi) - i\tau_y \sin(n\phi)\big], \tag{13}$$

$$\Omega_\phi^{LR} = \left(\frac{-in k_\rho^{n-1}}{2(\lambda - \omega_0)^3}\right)[\tau_x \cos(n\phi) + \tau_y \sin(n\phi)], \tag{14}$$

$$\Omega_z^{LR} = \left(\frac{n^2 k_\rho^{2(n-1)}}{2(\lambda - \omega_0)^3}\right)(k_z + i\tau_z), \tag{15}$$

for which we define the Berry connection as $\mathbf{A}^{LR} = i\langle\psi^L(\mathbf{k})|\nabla_{\mathbf{k}}|\psi^R(\mathbf{k})\rangle$. Upon integrating the Berry curvature on a closed surface containing the exceptional contour, one can analytically demonstrate that the total Berry charge is still real and quantized,

$$\gamma = \int_S \boldsymbol{\Omega}^{LR}(\mathbf{k}) \cdot d\mathbf{S} = n, \tag{16}$$

for which the full proof is given in Appendix. If the Berry curvature is integrated on a closed surface that does not enclose any portion of the exceptional contour, the resulting charge is zero [70]. Thus, as gain and loss are added to any topologically charged system, the topological charge is preserved on the exceptional contour that forms from the original topologically charged degeneracy.

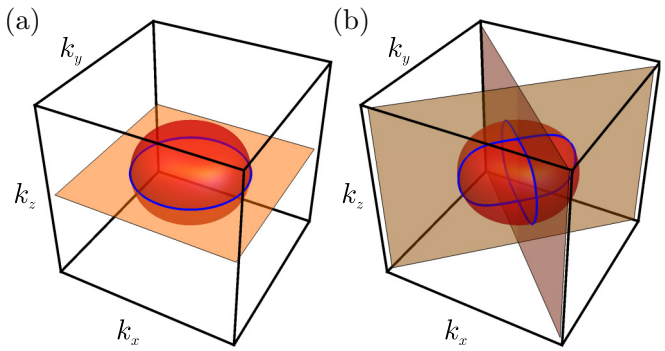

FIG. 2. (a) Exceptional contour associated with a charge-1 Weyl point under non-Hermitian perturbation, as described by Eq. (3) with $n = 1$ and $\boldsymbol{\tau} = (0,0,\tau_z)$. (b) Exceptional contour associated with a charge-2 Weyl point under non-Hermitian perturbation, as described by Eq. (3) with $n = 2$ and $\boldsymbol{\tau} = (\tau_x,0,0)$. In both panels, the two surfaces plotted are Eq. (5) (red) and Eq. (6) (orange), and their intersection defines the exceptional contour (blue).

Previous studies on the effects of adding non-Hermitian material to otherwise Hermitian systems with isolated degeneracies have focused on Dirac points and charge-1 Weyl points, for which the resulting exceptional contour in both cases is a ring [51,54,58,59], shown in Fig. 2(a). However, the general requirements for the formation of the exceptional contour, Eqs. (5) and (6), do not necessitate this outcome. For example, in a non-Hermitian system with an underlying charge-2 Weyl point described by Eq. (3) with $n = 2$ and $\boldsymbol{\tau} = (\tau_x,0,0)$, the resulting exceptional contour consists of two intersecting rings, and it is shown in Fig. 2(b).

It is worth remarking on the difference between adding a Hermitian versus non-Hermitian perturbation to a Hamiltonian containing a charge-n Weyl point, Eq. (1). The consequence of adding a general Hermitian perturbation to this Hamiltonian is to break the symmetry protecting the charge-n Weyl point, breaking up the single Weyl point into n charge-1 Weyl points. In contrast, upon adding a general anti-Hermitian perturbation of the form considered in Eq. (3), the charge-n Weyl point transforms into a single exceptional contour with charge n, rather than forming n charge-1 exceptional contours, a result that is guaranteed by the form of Eqs. (5) and (6). Moreover, a non-Hermitian perturbation can be used to reconstruct a single charge-n exceptional contour from n charge-1 Weyl points that have been split apart by a Hermitian perturbation.

C. A general criteria for forming exceptional contour in two-band systems

In Sec. II A, we derived the two criteria for finding an exceptional contour when a fixed amount of gain and loss is added to an underlying Hermitian system with a charge-n Weyl point in Eqs. (5) and (6). These two conditions can be generalized to a broader class of non-Hermitian Hamiltonians in which the added gain and loss is wave-vector-dependent, $\boldsymbol{\tau}(\mathbf{k})$. Consider a generic 2×2 non-Hermitian Hamiltonian,

$$H(\mathbf{k}) = f_x(\mathbf{k})\sigma_x + f_y(\mathbf{k})\sigma_y + f_z(\mathbf{k})\sigma_z + \omega_0 I, \tag{17}$$

in which the functions $f_i(\mathbf{k})$ are complex, smooth functions that describe the band structure. The upper and lower branches of the eigenvalues of this system can be written as

$$\lambda_\pm - \omega_0 = \pm\sqrt{f_x^2(\mathbf{k}) + f_y^2(\mathbf{k}) + f_z^2(\mathbf{k})} = \pm\sqrt{\det[H - \omega_0 I]}, \tag{18}$$

so that the general requirements for finding $\lambda_+ = \lambda_-$ are

$$\mathrm{Re}[\det[H - \omega_0 I]] = 0, \tag{19}$$

$$\mathrm{Im}[\det[H - \omega_0 I]] = 0. \tag{20}$$

Again, as there are only two constraints but three degrees of freedom, and thus absent some additional system symmetry that allows higher-dimensional surfaces to form, we expect to only find one-dimensional contours (i.e., lines) of exceptional points.

Moreover, these lines in parameter space where $\lambda_+ = \lambda_-$ are comprised entirely of exceptional points. To prove this, we first assume that our system is not at a point where $H(\mathbf{k}_0) - \omega_0 I = 0$. Then, we solve for the left and right eigenvectors of the generic non-Hermitian system in Eq. (17),

$$|\psi_\pm^R\rangle = (f_x(\mathbf{k}) - i f_y(\mathbf{k}),\ \lambda_\pm - \omega_0 - f_z(\mathbf{k}))^T, \tag{21}$$

$$\langle\psi_\pm^L| = (f_x(\mathbf{k}) + i f_y(\mathbf{k}),\ \lambda_\pm - \omega_0 - f_z(\mathbf{k})), \tag{22}$$

and then calculate their inner product,

$$\langle\psi_\pm^L|\psi_\pm^R\rangle = 2\det[H - \omega_0 I] \mp 2 f_z(\mathbf{k})\sqrt{\det[H - \omega_0 I]}. \tag{23}$$

As the condition for $\lambda_+ = \lambda_-$ is $\det[H(\mathbf{k}_0) - \omega_0 I] = 0$, at every point where these two eigenvalues are equal the eigenvectors are self-orthogonal, $\langle\psi_\pm^L|\psi_\pm^R\rangle = 0$, and so these lines in parameter space where the two eigenvalues are equal are guaranteed to be lines of exceptional points.

D. Topological phase transition induced by exceptional contour merging

In Hermitian systems with two bands, the only way to remove a Weyl point from the band structure is for it to combine with an oppositely charged Weyl point, after which the two bands develop a band gap. However, the addition of non-Hermitian terms to a system's Hamiltonian provides a different mechanism by which topological charge can be dissipated, when the exceptional contours with opposite topological charge merge to become a single, uncharged exceptional contour. To give a simple example of this phenomena, consider the system

$$H = k_x\sigma_x + k_y\sigma_y + \left(k_z^2 - k_0^2\right)\sigma_z + i\boldsymbol{\tau}\cdot\boldsymbol{\sigma}, \tag{24}$$

which contains two Weyl points with opposite charge at $k_z = \pm k_0$ for $\boldsymbol{\tau} = \mathbf{0}$. As gain and loss is added to the system with $\boldsymbol{\tau} = (0,\tau_y,0)$, each of these charge-1 Weyl points becomes a charge-1 Weyl exceptional contour, as can be seen in Fig. 3(a). But, as the strength of the gain and loss is increased, the two Weyl exceptional contours eventually touch at the threshold $\tau_y = k_0^2$, as shown in Fig. 3(b). When this happens, it becomes impossible to draw a surface over which to calculate the Berry charge that only contains a single exceptional contour, and as such the topological charge contained on each of the Weyl exceptional rings is dissipated, leaving a single uncharged exceptional contour, shown in Fig. 3(c). Interestingly, in this example, the topological charge can dissipate without opening a gap.

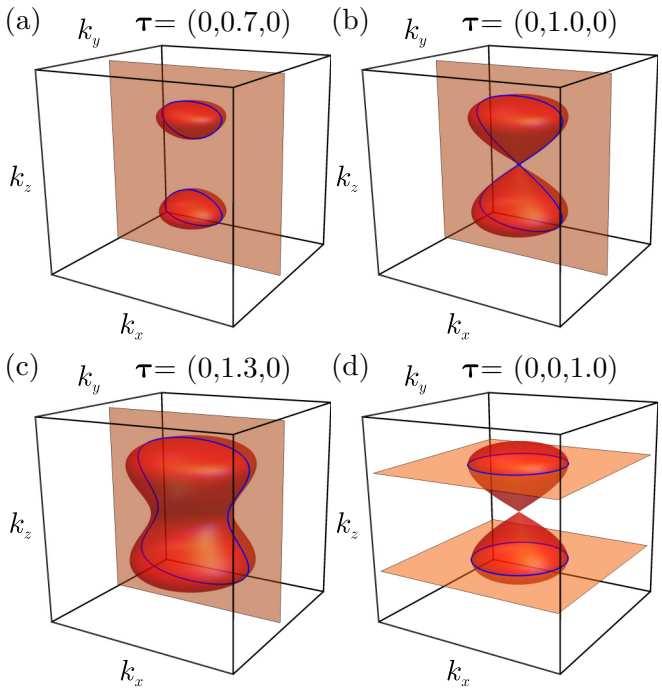

FIG. 3. Exceptional contours for the Hamiltonian of Eq. (24) with $k_0 = 1$. In all panels, the two surfaces plotted are Eq. (5) (red) and Eq. (6) (orange), and their intersection defines the exceptional contour (blue). (a) $\boldsymbol{\tau} = (0,0.7,0)$. (b) $\boldsymbol{\tau} = (0,1.0,0)$. At this value of $\boldsymbol{\tau}$, the exceptional contours touch, the Berry flux dissipates, and the exceptional contour become uncharged. (c) $\boldsymbol{\tau} = (0,1.3,0)$. (d) $\boldsymbol{\tau} = (0,0,1.0)$. Regardless of the strength of τ_z, the exceptional contours never merge for $\boldsymbol{\tau} = \tau_z$.

The existence of such a threshold is dependent upon the form of the non-Hermitian Hamiltonian. To illustrate this, in Fig. 3(d) we show the same system except with $\boldsymbol{\tau} = (0,0,\tau_z)$. As can be seen, the surfaces corresponding to the second criteria for finding the exceptional contour, Eq. (20), run parallel to one another, regardless of the value of τ_z. Thus, the two exceptional contours for this system for this distribution of gain and loss will never touch for any strength of the added gain and loss, and hence they will retain their topological charge.

E. Multiple exceptional contours

So far, we have focused on adding a constant strength of gain and loss to particular lattice sites. In this section, we briefly explore some of the additional complexities that can arise if the non-Hermitian perturbation to the system is dependent upon the wave vector, i.e., $\boldsymbol{\tau} = \boldsymbol{\tau}(\mathbf{k})$. In this case, it is possible to find that the intersection of Eqs. (19) and (20) yields multiple separate exceptional contours.

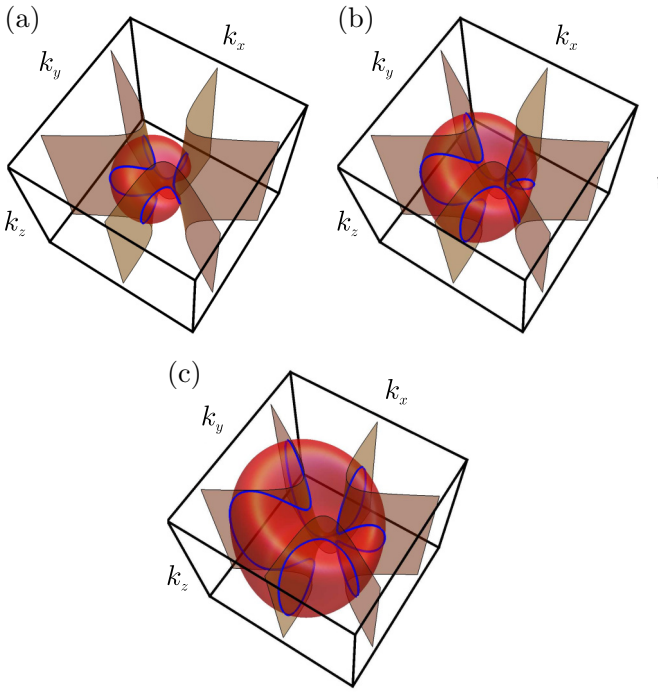

FIG. 4. Exceptional contour associated with a charge-2 Weyl point with wave-vector-dependent gain and loss added, as described by Eq. (3) with $n = 2$ and $\boldsymbol{\tau}(\mathbf{k}) = \tau_0(-4k_x + \sqrt{12}, -4k_y + 1, -1/\sqrt{2})$, with $\tau_0 = 0.7$ (a), $\tau_0 = 1.0$ (b), and $\tau_0 = 1.3$ (c). The two surfaces plotted are Eq. (19) (red) and Eq. (20) (orange), and their intersection defines the exceptional contour (blue). As can be seen, a portion of the exceptional contour splits off for $\tau_0 \sim 1$, yielding two independent exceptional contours. When this happens, the smaller exceptional contour does not carry a Berry charge, while the larger exceptional contour still carries a Berry charge of 2.

For example, consider the charge-2 system described by Eq. (3) with $\boldsymbol{\tau}(\mathbf{k}) = \tau_0(-4k_x + \sqrt{12}, -4k_y + 1, -1/\sqrt{2})$, in which τ_0 provides an overall scaling to the strength of the gain and loss. This system exhibits three distinct phases depending on the value of τ_0. First, for small values of τ_0, the system possesses a single exceptional contour with a Berry charge of 2, similar to the examples considered in previous sections and shown in Fig. 4(a). Next, as the strength of the gain and loss is increased beyond a threshold value, $\tau_0 \geqslant \tau_{2c}$, a second exceptional contour appears that is separate from the original Weyl exceptional contour, shown in Fig. 4(b). This second exceptional contour does not possess a Berry charge. Finally, as τ_0 is increased past a second threshold value, $\tau_0 \geqslant \tau_{1c}$, the two exceptional contours merge and form a single exceptional contour with charge 2, shown in Fig. 4(c). This example also illustrates that even when the added wave-vector-dependent gain and loss breaks some of the symmetries of the underlying Hermitian system, the entire quantized Berry charge of the system can still be found on a single exceptional contour. In this example, when $\tau_0 = 0$, the charge-2 Weyl point in H is protected by C_4 symmetry, but this is not true for $\tau_0 \neq 0$, and the resulting exceptional contour still has a Berry charge of 2, rather than splitting into two charge-1 exceptional contours.

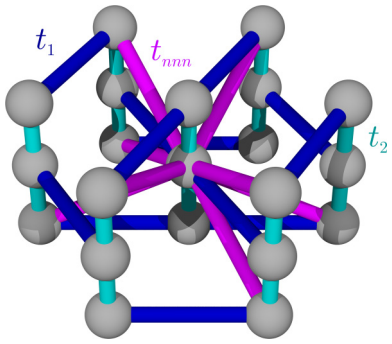

FIG. 5. Schematic of the tight-binding model for a metallic chiral woodpile photonic crystal [71]. The nearest-neighbor bonds are shown in blue (t_{n1}) and cyan (t_{n2}), while the next-nearest-neighbor bonds connected to the center site are shown in purple (t_{nnn}).

Note that in choosing to add a wave-vector-dependent non-Hermitian perturbation to the system, we stipulate that as each $k_i \to \pm\infty$, the Hermitian portion of the Hamiltonian should dominate the behavior of the system, so that the non-Hermitian addition can still be considered a perturbation on the underlying Hermitian system. To satisfy this criterion and still be able to add a wave-vector-dependent non-Hermitian term to the system, the minimum charge of the Weyl point in the underlying Hermitian system is 2.

III. PHOTONIC REALIZATIONS OF WEYL EXCEPTIONAL CONTOURS

In the previous section, using a two-band effective Hamiltonian, we describe a number of interesting effects when a non-Hermitian perturbation is added to a topologically nontrivial Hermitian Hamiltonian supporting Weyl points. These effects include the formation of topologically charged exceptional contours with unusual shapes and the dissipation of topological charge without opening a band gap. In this section, we will show that these novel physical effects can be realized in realistic photonic systems.

To observe a nonring Weyl exceptional contour, we use a metallic chiral woodpile photonic crystal designed to operate in the terahertz frequency band, for which the underlying Hermitian system can possess charge-2 Weyl points. The details of the structure can be found in Ref. [71]. For the purposes of this paper, following [71], we note that the properties of this structure are well described by the tight-binding model as shown in Fig. 5. The model consists of layers of a hexagonal lattice directly on top of each other. The lattice sites (gray spheres) are connected by nearest-neighbor hopping, intralayer hopping along only one of the lattice vector directions with strength t_{n1}, shown as blue bonds in Fig. 5, and interlayer hopping with strength t_{n2}, shown as cyan bonds in Fig. 5. In addition, there is a set of next-nearest-neighbor hopping terms, with strength t_{nnn}, and all of these bonds connected to the central lattice site in Fig. 5 are shown as purple bonds. The tight-binding Hamiltonian for this system is

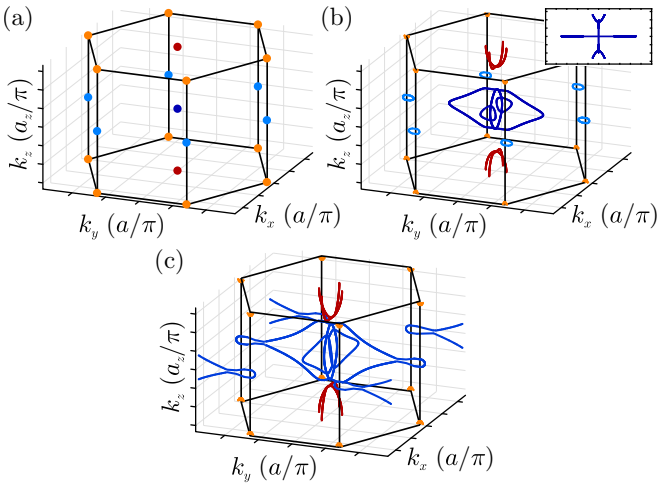

FIG. 6. Plot of the (a) Weyl points and (b),(c) Weyl exceptional contours of the tight-binding model given in Eq. (25) with hopping strengths $t_{n1} = 1$, $t_{n2} = -1$, and $t_{\mathrm{nnn}} = 0.2$. In (b), gain and loss has been added to two of the three lattice sites in the unit cell, with $\varepsilon_1 = \varepsilon_3^* = 0.2i$ and $\varepsilon_2 = 0$. The two charge-2 Weyl points and exceptional contours at Γ and A are shown in dark blue and dark red, respectively, while the numerous charge-1 Weyl points and exceptional contours at K and H are shown in light blue and orange. A top-down view of the charge-2 Weyl exceptional contour at Γ is shown in the inset. In (c), sufficient gain and loss has been added, $\varepsilon_1 = \varepsilon_3^* = 0.29i$, to cause the charge-2 Weyl exceptional contour at Γ to merge with two of the charge-1 Weyl exceptional contours at K, forming a single uncharged exceptional contour.

then

$$H = \sum_{i,k} \varepsilon_k a_{i,k}^\dagger a_{i,k} + \sum_{\langle i,j\rangle} t_{n1} a_{i,k}^\dagger a_{j,k} + \text{c.c.} + \sum_{i,k} t_{n2} a_{i,k}^\dagger a_{i,k+1} + \text{c.c.} + \sum_{\langle\langle i,j\rangle\rangle} t_{nnn} a_{i,k}^\dagger a_{j,k+1} + \text{c.c.}, \tag{25}$$

in which $a_{i,k}$ and $a_{i,k}^\dagger$ are the annihilation and creation operators at the ith lattice site within the kth lattice layer, $\langle i,j\rangle$ denotes a pair of intralayer nearest neighbors, and $\langle\langle i,j\rangle\rangle$ denotes a pair of interlayer next-nearest-neighbor couplings. If we set $t_{n1} = 1$, $t_{n2} = -1$, and $t_{\mathrm{nnn}} = 0.2$, this three-band model contains a charge-2 Weyl point between two bands at Γ and a set of charge-1 Weyl points between the same bands at K, such that the total Berry charge in the $k_z = 0$ plane is zero. Likewise, a second charge-2 Weyl point can be found at A alongside charge-1 Weyl points at H, again such that there is no net Berry charge in the $k_z = \pm\pi/2$ plane [71].

To break hermiticity in the system, we allow the on-site energies in each lattice layer to be complex, $\varepsilon_k \in \mathbb{C}$, which corresponds to adding gain or loss to that layer of the photonic crystal. The resulting Weyl exceptional contours in this system are shown in Fig. 6, in which the exceptional contour stemming from the charge-2 Weyl point at A resembles two intersecting rings, which is similar to the shape of the charge-2 Weyl exceptional contour considered in Fig. 2(b). The charge-2 Weyl exceptional contour at Γ consists of four interlocking rings. The larger two rings are centered at Γ, while the smaller two rings are situated opposite one another in k_x, demonstrating that additional complexities are possible in realistic systems beyond the simple systems considered in Sec. II. A top-down view of the charge-2 Weyl exceptional contour at Γ is shown in the inset of Fig. 6(b). Additional charge-1 Weyl exceptional rings are seen at K and H. The quantization of the Berry charge for all of these Weyl exceptional contours is confirmed numerically.

As the gain and loss in this system is further increased, the topologically charged exceptional contours begin to merge together to form topologically trivial exceptional contours, in agreement with the systems considered in Sec. II D. In Fig. 6(c), the charge-2 Weyl exceptional contour at Γ has merged with two of the charge-1 Weyl exceptional contours at K to form a single uncharged exceptional contour.

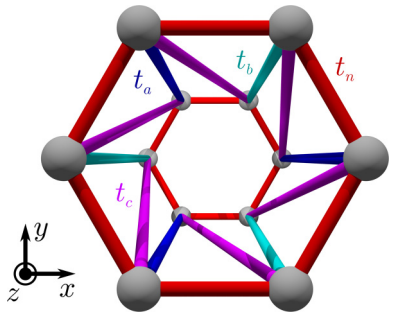

FIG. 7. Schematic of the tight-binding model for the Hamiltonian given in Eq. (29), which can be realized in both acoustic [23] and photonic [26] systems. The intralayer bonds with strength t_n are red, the direct interlayer bonds for the A and B sites are t_a (blue) and t_b (cyan), respectively, and the interlayer next-nearest-neighbor bonds, t_c, are shown in purple.

IV. CHIRAL EDGE MODES

One of the most important properties of Hermitian Weyl semimetals are their surface states, which allow for one-way transport. As such, it is of critical importance to understand whether surface states persist in non-Hermitian topological systems, and if so how they are effected by the presence of the gain and loss. Here we study a non-Hermitian extension of a three-dimensional Hermitian system exhibiting a charge-1 Weyl point [72], and we demonstrate that surface states of this system are preserved outside of the Weyl exceptional contour.

The non-Hermitian three-dimensional model we consider consists of layers of a stacked honeycomb lattice, in which all layers are directly stacked on top of each other, as shown in Fig. 7. The Hamiltonian reads

$$H_\perp = \sum_{i,m} \varepsilon_a a_{i,m}^\dagger a_{i,m} + \varepsilon_b b_{i,m}^\dagger b_{i,m} + \sum_{\langle i,j\rangle,m} t_n (a_{i,m}^\dagger b_{j,m} + b_{j,m}^\dagger a_{i,m}). \tag{26}$$

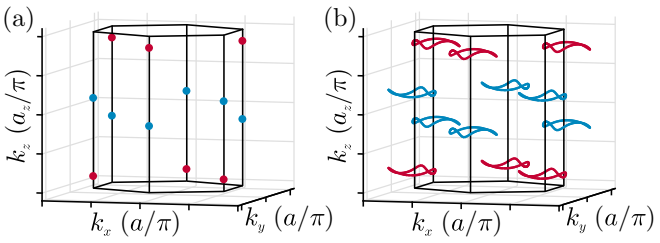

FIG. 8. Locations of Weyl points (a) and Weyl exceptional rings (b) for the Hamiltonian given in Eq. (29) with $t_a = -t_b = 4$, $t_c = 3$, and $t_n = 10$. In (b), gain and loss have been added to the A and B sites of the lattice, with $\varepsilon_a = \varepsilon_b^* = 9i$.

Here, $a_{i,m}$,$b_{i,m}$ are the annihilation operators at the ith site on the mth layer of the two sublattices of the honeycomb crystal. The on-site energies of the two sublattices are $\varepsilon_{a,b}$, the in-plane coupling strength is t_n, and $\langle i,j\rangle$ represents a pair of nearest neighbors. In addition, there are two forms of out-of-plane couplings, direct coupling between neighboring layers,

$$H_D = \sum_{i,m} t_a a^\dagger_{i,m+1} a_{i,m} + t_b b^\dagger_{i,m+1} b_{i,m} + \text{c.c.}, \tag{27}$$

and coupling between next-nearest neighbors on adjacent layers,

$$H_{\text{NNN}} = \sum_{\langle\langle i,j\rangle\rangle,m} t_c (a^\dagger_{i,m+1} a_{j,m} + b^\dagger_{i,m+1} b_{j,m}) + \text{c.c.}, \tag{28}$$

in which $\langle\langle i,j\rangle\rangle$ represents the possible pairs of interlayer next-nearest neighbors. These three different couplings are shown schematically in Fig. 7. Together, the total system,

$$H_0 = H_\perp + H_D + H_{\text{NNN}}, \tag{29}$$

contains a set of Weyl points whose positions depend upon the choice of the coupling strength parameters [23]. This Hamiltonian has been previously shown to be realizable either in acoustic systems [23] or in a photonic system using the concept of synthetic dimensions [26].

To break hermiticity in this system, gain and loss are added to the two on-site energies, and they are chosen such that $\varepsilon_b = \varepsilon_a^*$ to enforce that an equal amount of gain and loss is added to the two lattice sites. In doing so, each of the charge-1 Weyl points in the underlying Hermitian system turns into a Weyl exceptional ring, as shown in Fig. 8. As the strength of the gain and loss is increased, these exceptional rings are no longer centered on the original Weyl points of the underlying Hermitian system.

The consequences of these changes can be seen in the surface states of the surface formed by cutting through all of the layers along a zigzag edge at the same in-plane location, i.e., the cut is made parallel to the z axis as defined in Fig. 7. The band structures for a semi-infinite system containing two such surfaces along the x axis are shown in Fig. 9 for a plane of constant k_z, for four different choices of k_z. First, when k_z is below the exceptional contour, the upper and lower bands are separated by a topologically trivial gap, and no topologically protected surface states are seen [Fig. 9(b)]. As k_z approaches the exceptional contour, the upper and lower bands begin to overlap within the region where the exceptional contour forms [Fig. 9(c)]. When k_z is within the the exceptional contour, some of the lower bulk bands cross over through the exceptional contour to the upper band, and vice versa, as seen in Fig. 9(d). This crossover of the bulk bands is the manifestation of the intersecting sheets of the Riemann surface topology between the branch points that comprise the exceptional contour, as exemplified in Figs. 1(b) and 1(c). Finally, when k_z is increased past the entire exceptional contour, a topologically nontrivial gap opens between the upper and lower bands. Within this gap there are topologically protected surface states. These states have nonzero imaginary components in their eigenvalues, indicating the novel possibility of one-way amplification or dissipation in these systems.

V. CONCLUSION

In conclusion, we have provided a systematic study of the effects of introducing non-hermiticity to topologically charged systems. In doing so, we have proven that a Weyl point with arbitrary charge in a Hermitian system transforms into a one-dimensional exceptional contour on which the topological charge is preserved. Moreover, we have shown that the addition of gain and loss may result in a new class of topological phase transition, through which the topological charge can dissipate without opening a gap. Our results highlight significant opportunities for exploring topological physics in non-Hermitian systems.

ACKNOWLEDGMENTS

This work was supported by an AFOSR MURI program (Grant No. FA9550-12-1-0471) and an AFOSR project (Grant No. FA9550-16-1-0010).

APPENDIX: PROOF OF THE QUANTIZED BERRY CHARGE

In this appendix, we provide an analytic proof that the exceptional contour in the non-Hermitian Hamiltonian given in Eq. (3) still possesses a quantized topological charge identical to that of the charge of the Weyl point in the underlying Hermitian system when $\boldsymbol{\tau} = \mathbf{0}$. To begin, we choose a closed cylinder in wave-vector space as our surface of integration, with radius R and height $2Z$ centered at the origin. Additionally, we require that $R^{2n} > \boldsymbol{\tau}^2$ and $Z^2 > \boldsymbol{\tau}^2$ so that the resulting closed cylinder contains the entire exceptional contour. The total topological charge of the system is then given by

$$\gamma = \int_0^{2\pi} \left[\int_0^R k_\rho \Omega_z^{LR}|_{k_z=Z} dk_\rho + R \int_{-Z}^{Z} \Omega_\rho^{LR}|_{k_\rho=R} dk_z - \int_0^R k_\rho \Omega_z^{LR}|_{k_z=-Z} dk_\rho \right] d\phi, \tag{A1}$$

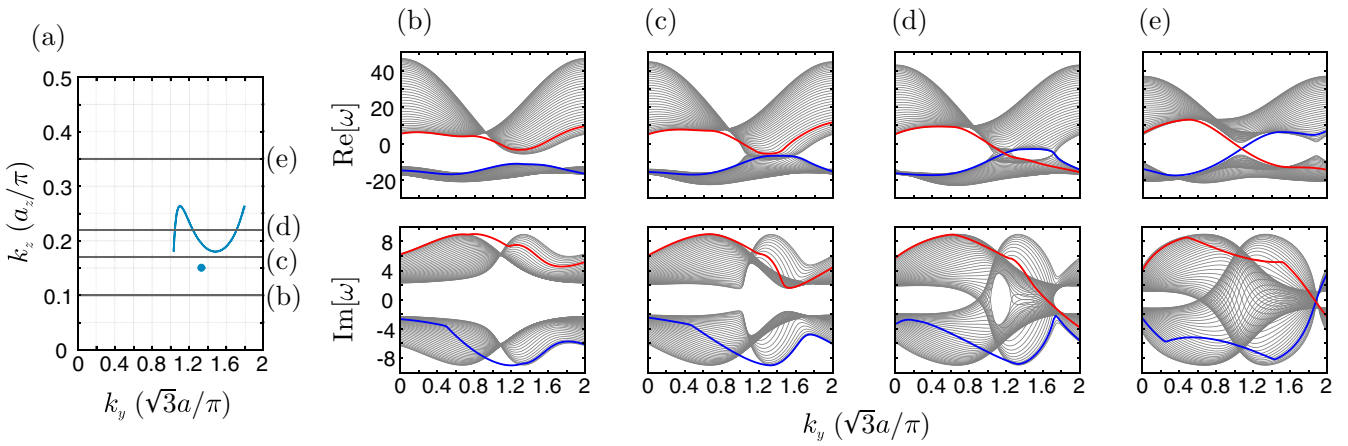

FIG. 9. (a) Projection of the Weyl point (solid circle) of the underlying Hermitian system given in Eq. (29) and the exceptional contour of the full non-Hermitian system in the k_y–k_z plane, with $t_a = -t_b = 4$, $t_c = 3$, $t_n = 10$, and $\varepsilon_a = \varepsilon_b^* = 9i$. The four gray lines denote the value of k_z chosen to calculate the band structure in plots (b)–(e). (b) k_z is below the exceptional contour, and the upper and lower bands are separated by a topologically trivial gap, so no topologically protected surface states are seen. (c) As k_z approaches the exceptional contour, the upper and lower bands overlap within the region where the exceptional contour forms. (d) k_z is in the middle of the exceptional contour, and some of the lower bands cross over to become upper bands within the exceptional contour, and vice versa. (e) k_z is greater than the entire exceptional contour, and thus a topologically nontrivial gap opens between the upper and lower bands. In (b)–(d), the blue and red states correspond to surface states that are not topologically protected, while in (e) these two states correspond to the topologically protected surface states.

i.e., the integrals are over the top base, the side, and bottom base of the closed cylinder, respectively. Note that the minus sign in the third term comes from $d\mathbf{S} = -\hat{z}$ on the bottom base. The integrals over k_z and k_ρ can be directly evaluated as

$$\int_0^R k_\rho \Omega_z^{LR}|_{k_z=Z} dk_\rho = \left(\frac{n}{2}\right)\left(\frac{Z + i\tau_z}{Z^2 - \boldsymbol{\tau}^2 + 2i\tau_z Z + [\tau_x \cos(n\phi) - \tau_y \sin(n\phi)]^2}\right) \times \left[\sqrt{Z^2 - \boldsymbol{\tau}^2 + 2i\tau_z Z} - \frac{Z^2 - \boldsymbol{\tau}^2 + 2i\tau_z Z + iR^n[\tau_x \cos(n\phi) - \tau_y \sin(n\phi)]}{\sqrt{R^{2n} + Z^2 - \boldsymbol{\tau}^2 + 2i[\tau_x \cos(n\phi) - \tau_y \sin(n\phi)] + 2i\tau_z Z}}\right], \tag{A2}$$

$$R\int_{-Z}^{Z} \Omega_\rho^{LR}|_{k_\rho=R} dk_z = \left(\frac{n}{2}\right)\left(\frac{R^{2n} + iR^n[\tau_x \cos(n\phi) - \tau_y \sin(n\phi)]}{R^{2n} - \tau_x^2 - \tau_y^2 + 2iR^n[\tau_x \cos(n\phi) - \tau_y \sin(n\phi)]}\right) \times \left[\frac{Z + i\tau_z}{\sqrt{R^{2n} + Z^2 - \boldsymbol{\tau}^2 + 2i[\tau_x \cos(n\phi) - \tau_y \sin(n\phi)] + 2i\tau_z Z}} + \frac{Z - i\tau_z}{\sqrt{R^{2n} + Z^2 - \boldsymbol{\tau}^2 + 2i[\tau_x \cos(n\phi) - \tau_y \sin(n\phi)] - 2i\tau_z Z}}\right], \tag{A3}$$

with the integral over the bottom base being identical to that of Eq. (A2), except with $Z \to -Z$.

Next, before evaluating the integral over ϕ, we let $R \to \infty$, and we keep only the leading-order nonzero terms. In doing so, Eq. (A3) becomes zero immediately. In addition, the denominator of the second term in the square brackets of Eq. (A2) can be simply replaced by R^n, and hence its contribution to the integral over ϕ vanishes. The integration of Eq. (A2) over the azimuthal angle ϕ can now be evaluated using Cauchy's residue theorem, which evaluates to $n/2$. Thus, upon combining the contributions from both the top and bottom of the closed surface, we find that $\gamma = n$, completing the proof.

[1] C. L. Kane and E. J. Mele, Quantum Spin Hall Effect in Graphene, Phys. Rev. Lett. **95**, 226801 (2005).
[2] M. König, S. Wiedmann, C. Brüne, A. Roth, H. Buhmann, L. W. Molenkamp, X.-L. Qi, and S.-C. Zhang, Quantum spin Hall insulator state in HgTe quantum wells, Science **318**, 766 (2007).
[3] F. D. M. Haldane and S. Raghu, Possible Realization of Directional Optical Waveguides in Photonic Crystals with Broken Time-Reversal Symmetry, Phys. Rev. Lett. **100**, 013904 (2008).
[4] D. Hsieh, D. Qian, L. Wray, Y. Xia, Y. S. Hor, R. J. Cava, and M. Z. Hasan, A topological Dirac insulator in a quantum spin Hall phase, Nature (London) **452**, 970 (2008).
[5] S. Raghu and F. D. M. Haldane, Analogs of quantum-Hall-effect edge states in photonic crystals, Phys. Rev. A **78**, 033834 (2008).
[6] Z. Wang, Y. Chong, J. D. Joannopoulos, and M. Soljačić, Observation of unidirectional backscattering-immune topological electromagnetic states, Nature (London) **461**, 772 (2009).

[7] J. Koch, A. A. Houck, K. L. Hur, and S. M. Girvin, Time-reversal-symmetry breaking in circuit-QED-based photon lattices, Phys. Rev. A **82**, 043811 (2010).

[8] R. O. Umucalılar and I. Carusotto, Artificial gauge field for photons in coupled cavity arrays, Phys. Rev. A **84**, 043804 (2011).

[9] M. Hafezi, E. A. Demler, M. D. Lukin, and J. M. Taylor, Robust optical delay lines with topological protection, Nat. Phys. **7**, 907 (2011).

[10] K. Fang, Z. Yu, and S. Fan, Realizing effective magnetic field for photons by controlling the phase of dynamic modulation, Nat. Photon. **6**, 782 (2012).

[11] Y. E. Kraus, Y. Lahini, Z. Ringel, M. Verbin, and O. Zilberberg, Topological States and Adiabatic Pumping in Quasicrystals, Phys. Rev. Lett. **109**, 106402 (2012).

[12] T. Kitagawa, M. A. Broome, A. Fedrizzi, M. S. Rudner, E. Berg, I. Kassal, A. Aspuru-Guzik, E. Demler, and A. G. White, Observation of topologically protected bound states in photonic quantum walks, Nat. Commun. **3**, 1872 (2012).

[13] M. C. Rechtsman, J. M. Zeuner, Y. Plotnik, Y. Lumer, D. Podolsky, F. Dreisow, S. Nolte, M. Segev, and A. Szameit, Photonic Floquet topological insulators, Nature (London) **496**, 196 (2013).

[14] A. B. Khanikaev, S. Hossein Mousavi, W.-K. Tse, M. Kargarian, A. H. MacDonald, and G. Shvets, Photonic topological insulators, Nat. Mater. **12**, 233 (2013).

[15] M. Hafezi, S. Mittal, J. Fan, A. Migdall, and J. M. Taylor, Imaging topological edge states in silicon photonics, Nat. Photon. **7**, 1001 (2013).

[16] X. Wan, A. M. Turner, A. Vishwanath, and S. Y. Savrasov, Topological semimetal and Fermi-arc surface states in the electronic structure of pyrochlore iridates, Phys. Rev. B **83**, 205101 (2011).

[17] K.-Y. Yang, Y.-M. Lu, and Y. Ran, Quantum Hall effects in a Weyl semimetal: Possible application in pyrochlore iridates, Phys. Rev. B **84**, 075129 (2011).

[18] L. Lu, L. Fu, J. D. Joannopoulos, and M. Soljačić, Weyl points and line nodes in gyroid photonic crystals, Nat. Photon. **7**, 294 (2013).

[19] S.-Y. Xu, I. Belopolski, N. Alidoust, M. Neupane, G. Bian, C. Zhang, R. Sankar, G. Chang, Z. Yuan, C.-C. Lee, S.-M. Huang, H. Zheng, J. Ma, D. S. Sanchez, B. Wang, A. Bansil, F. Chou, P. P. Shibayev, H. Lin, S. Jia, and M. Z. Hasan, Discovery of a Weyl fermion semimetal and topological Fermi arcs, Science **349**, 613 (2015).

[20] B. Q. Lv, N. Xu, H. M. Weng, J. Z. Ma, P. Richard, X. C. Huang, L. X. Zhao, G. F. Chen, C. E. Matt, F. Bisti, V. N. Strocov, J. Mesot, Z. Fang, X. Dai, T. Qian, M. Shi, and H. Ding, Observation of Weyl nodes in TaAs, Nat. Phys. **11**, 724 (2015).

[21] L. X. Yang, Z. K. Liu, Y. Sun, H. Peng, H. F. Yang, T. Zhang, B. Zhou, Y. Zhang, Y. F. Guo, M. Rahn, D. Prabhakaran, Z. Hussain, S.-K. Mo, C. Felser, B. Yan, and Y. L. Chen, Weyl semimetal phase in the non-centrosymmetric compound TaAs, Nat. Phys. **11**, 728 (2015).

[22] A. A. Soluyanov, D. Gresch, Z. Wang, Q. S. Wu, M. Troyer, X. Dai, and B. A. Bernevig, Type-II Weyl semimetals, Nature (London) **527**, 495 (2015).

[23] M. Xiao, W.-J. Chen, W.-Y. He, and C. T. Chan, Synthetic gauge flux and Weyl points in acoustic systems, Nat. Phys. **11**, 920 (2015).

[24] L. Lu, C. Fang, L. Fu, S. G. Johnson, J. D. Joannopoulos, and M. Soljačić, Symmetry-protected topological photonic crystal in three dimensions, Nat. Phys. **12**, 337 (2016).

[25] W.-J. Chen, M. Xiao, and C. T. Chan, Photonic crystals possessing multiple Weyl points and the experimental observation of robust surface states, Nat. Commun. **7**, 13038 (2016).

[26] Q. Lin, M. Xiao, L. Yuan, and S. Fan, Photonic Weyl point in a two-dimensional resonator lattice with a synthetic frequency dimension, Nat. Commun. **7**, 13731 (2016).

[27] M. Xiao, Q. Lin, and S. Fan, Hyperbolic Weyl Point in Reciprocal Chiral Metamaterials, Phys. Rev. Lett. **117**, 057401 (2016).

[28] W. Gao, B. Yang, M. Lawrence, F. Fang, B. Bri, and S. Zhang, Photonic Weyl degeneracies in magnetized plasma, Nat. Commun. **7**, 12435 (2016).

[29] C. Fang, L. Lu, J. Liu, and L. Fu, Topological semimetals with helicoid surface states, Nat. Phys. **12**, 936 (2016).

[30] J. Noh, S. Huang, D. Leykam, Y. D. Chong, K. P. Chen, and M. C. Rechtsman, Experimental observation of optical Weyl points and Fermi arc-like surface states, Nat. Phys. **13**, 611 (2017).

[31] M. V. Berry, Quantal phase factors accompanying adiabatic changes, Proc. R. Soc. London, Ser. A **392**, 45 (1984).

[32] N. Bachelard, J. Andreasen, S. Gigan, and P. Sebbah, Taming Random Lasers Through Active Spatial Control of the Pump, Phys. Rev. Lett. **109**, 033903 (2012).

[33] T. Hisch, M. Liertzer, D. Pogany, F. Mintert, and S. Rotter, Pump-Controlled Directional Light Emission from Random Lasers, Phys. Rev. Lett. **111**, 023902 (2013).

[34] H. Hodaei, M.-A. Miri, M. Heinrich, D. N. Christodoulides, and M. Khajavikhan, Parity-time-symmetric microring lasers, Science **346**, 975 (2014).

[35] L. Feng, Z. J. Wong, R.-M. Ma, Y. Wang, and X. Zhang, Single-mode laser by parity-time symmetry breaking, Science **346**, 972 (2014).

[36] S. F. Liew, B. Redding, L. Ge, G. S. Solomon, and H. Cao, Active control of emission directionality of semiconductor microdisk lasers, Appl. Phys. Lett. **104**, 231108 (2014).

[37] S. F. Liew, L. Ge, B. Redding, G. S. Solomon, and H. Cao, Pump-controlled modal interactions in microdisk lasers, Phys. Rev. A **91**, 043828 (2015).

[38] A. Cerjan, B. Redding, L. Ge, S. F. Liew, H. Cao, and A. Douglas Stone, Controlling mode competition by tailoring the spatial pump distribution in a laser: A resonance-based approach, Opt. Express **24**, 26006 (2016).

[39] A. Guo, G. J. Salamo, D. Duchesne, R. Morandotti, M. Volatier-Ravat, V. Aimez, G. A. Siviloglou, and D. N. Christodoulides, Observation of $\mathcal{PT}$-Symmetry Breaking in Complex Optical Potentials, Phys. Rev. Lett. **103**, 093902 (2009).

[40] A. Cerjan and S. Fan, Eigenvalue dynamics in the presence of nonuniform gain and loss, Phys. Rev. A **94**, 033857 (2016).

[41] M. Liertzer, L. Ge, A. Cerjan, A. D. Stone, H. E. Türeci, and S. Rotter, Pump-Induced Exceptional Points in Lasers, Phys. Rev. Lett. **108**, 173901 (2012).

[42] M. Brandstetter, M. Liertzer, C. Deutsch, P. Klang, J. Schöberl, H. E. Türeci, G. Strasser, K. Unterrainer, and S. Rotter, Reversing the pump dependence of a laser at an exceptional point, Nat. Commun. **5**, 4034 (2014).

[43] B. Peng, Ş. K. Özdemir, S. Rotter, H. Yilmaz, M. Liertzer, F. Monifi, C. M. Bender, F. Nori, and L. Yang, Loss-induced suppression and revival of lasing, Science **346**, 328 (2014).

[44] M. Lawrence, N. Xu, X. Zhang, L. Cong, J. Han, W. Zhang, and S. Zhang, Manifestation of $\mathcal{PT}$ Symmetry Breaking in Polarization Space With Terahertz Metasurfaces, Phys. Rev. Lett. **113**, 093901 (2014).

[45] A. Cerjan and S. Fan, Achieving Arbitrary Control Over Pairs of Polarization States Using Complex Birefringent Metamaterials, Phys. Rev. Lett. **118**, 253902 (2017).

[46] K. Esaki, M. Sato, K. Hasebe, and M. Kohmoto, Edge states and topological phases in non-Hermitian systems, Phys. Rev. B **84**, 205128 (2011).

[47] Y. C. Hu and T. L. Hughes, Absence of topological insulator phases in non-Hermitian $\mathcal{PT}$-symmetric Hamiltonians, Phys. Rev. B **84**, 153101 (2011).

[48] S. Malzard, C. Poli, and H. Schomerus, Topologically Protected Defect States in Open Photonic Systems with Non-Hermitian Charge-Conjugation and Parity-Time Symmetry, Phys. Rev. Lett. **115**, 200402 (2015).

[49] T. E. Lee, Anomalous Edge State in a Non-Hermitian Lattice, Phys. Rev. Lett. **116**, 133903 (2016).

[50] D. Leykam, K. Y. Bliokh, C. Huang, Y. D. Chong, and F. Nori, Edge Modes, Degeneracies, and Topological Numbers in Non-Hermitian Systems, Phys. Rev. Lett. **118**, 040401 (2017).

[51] Y. Xu, S.-T. Wang, and L.-M. Duan, Weyl Exceptional Rings in a Three-Dimensional Dissipative Cold Atomic Gas, Phys. Rev. Lett. **118**, 045701 (2017).

[52] W. Hu, H. Wang, P. P. Shum, and Y. D. Chong, Exceptional points in a non-Hermitian topological pump, Phys. Rev. B **95**, 184306 (2017).

[53] S. Weimann, M. Kremer, Y. Plotnik, Y. Lumer, S. Nolte, K. G. Makris, M. Segev, M. C. Rechtsman, and A. Szameit, Topologically protected bound states in photonic parity-time-symmetric crystals, Nat. Mater. **16**, 433 (2017).

[54] H. Shen, B. Zhen, and L. Fu, Topological band theory for non-Hermitian Hamiltonians, arXiv:1706.07435.

[55] C. M. Bender, S. Boettcher, and P. N. Meisinger, PT-symmetric quantum mechanics, J. Math. Phys. **40**, 2201 (1999).

[56] C. M. Bender, D. C. Brody, and H. F. Jones, Complex Extension of Quantum Mechanics, Phys. Rev. Lett. **89**, 270401 (2002).

[57] K. G. Makris, R. El-Ganainy, D. N. Christodoulides, and Z. H. Musslimani, Beam Dynamics in $\mathcal{PT}$ Symmetric Optical Lattices, Phys. Rev. Lett. **100**, 103904 (2008).

[58] A. Szameit, M. C. Rechtsman, O. Bahat-Treidel, and M. Segev, $\mathcal{PT}$-symmetry in honeycomb photonic lattices, Phys. Rev. A **84**, 021806(R) (2011).

[59] B. Zhen, C. W. Hsu, Y. Igarashi, L. Lu, I. Kaminer, A. Pick, S.-L. Chua, J. D. Joannopoulos, and M. Soljačić, Spawning rings of exceptional points out of Dirac cones, Nature (London) **525**, 354 (2015).

[60] A. Cerjan, A. Raman, and S. Fan, Exceptional Contours and Band Structure Design in Parity-Time Symmetric Photonic Crystals, Phys. Rev. Lett. **116**, 203902 (2016).

[61] A. Mock, Parity-time–symmetry breaking in two-dimensional photonic crystals: Square lattice, Phys. Rev. A **93**, 063812 (2016).

[62] A. Cerjan and S. Fan, Effects of non-uniform distributions of gain and loss in photonic crystals, New J. Phys. **18**, 125007 (2016).

[63] A. Mock, Characterization of parity-time symmetry in photonic lattices using Heesh-Shubnikov group theory, Opt. Express **24**, 22693 (2016).

[64] T. Kato, *Perturbation Theory for Linear Operators*, 2nd ed. (Springer, Berlin, 1995).

[65] W. D. Heiss, Exceptional points of non-Hermitian operators, J. Phys. A **37**, 2455 (2004).

[66] W. D. Heiss, The physics of exceptional points, J. Phys. A **45**, 444016 (2012).

[67] L. Ge and A. D. Stone, Parity-Time Symmetry Breaking Beyond One Dimension: The Role of Degeneracy, Phys. Rev. X **4**, 031011 (2014).

[68] C. Fang, M. J. Gilbert, X. Dai, and B. A. Bernevig, Multi-Weyl Topological Semimetals Stabilized by Point Group Symmetry, Phys. Rev. Lett. **108**, 266802 (2012).

[69] J. von Neumann and E. Wigner, On some peculiar discrete eigenvalues, Phys. Z. **30**, 467 (1929).

[70] As an exceptional point represents a singularity of the system where the two branches of λ coalesce and there is only a single, self-orthogonal eigenvector, it remains an open question how to properly define the Berry connection and curvature at these points. Therefore, in this paper, we do not consider the case in which the integration surface intersects with the contour.

[71] M.-L. Chang, M. Xiao, W.-J. Chen, and C. T. Chan, Multiple Weyl points and the sign change of their topological charges in woodpile photonic crystals, Phys. Rev. B **95**, 125136 (2017).

[72] F. D. M. Haldane, Model For a Quantum Hall Effect Without Landau Levels: Condensed-Matter Realization of the "Parity Anomaly,"Phys. Rev. Lett. **61**, 2015 (1988).